Interactive Snow Avalanche Segmentation from Webcam Imagery: results, potential and limitations

Elisabeth D. Hafner[1,2,3], Theodora Kontogianni[3,4], Rodrigo Caye Daudt[3], Lucien Oberson[1,2,5], Jan Dirk Wegner[3,6], Konrad Schindler[3], and Yves Bühler[1,2]

[1]WSL Institute for Snow and Avalanche Research SLF, Davos Dorf, 7260 Switzerland
[2]Climate Change, Extremes, and Natural Hazards in Alpine Regions Research Center CERC, Davos Dorf, 7260 Switzerland
[3]EcoVision Lab, Photogrammetry and Remote Sensing, ETH Zurich, Zurich, 8093 Switzerland
[4]ETH AI Center, ETH Zurich, Zurich, 8092 Switzerland
[5]Swiss National Railway, SBB, Berne, 3000 Switzerland
[6]Department of Mathematical Modeling and Machine Learning, University of Zurich, Zurich, 8057 Switzerland

Correspondence: Elisabeth D. Hafner (elisabeth.hafner@slf.ch)

Abstract.

For many safety-related applications such as hazard mapping or road management, well documented avalanche events are crucial. Nowadays, despite research into different directions, the available data is mostly restricted to isolated locations where it is collected by observers in the field. Webcams are becoming more frequent in the Alps and beyond, capturing numerous avalanche prone slopes. To complement the knowledge about avalanche occurrences, we propose to make use of this webcam imagery for avalanche mapping. For humans, avalanches are relatively easy to identify, but the manual mapping of their outlines is time intensive. Therefore, we propose to support the mapping of avalanches in images with a learned segmentation model. In interactive avalanche segmentation (IAS), a user collaborates with a deep learning model to segment the avalanche outlines, taking advantage of human expert knowledge while keeping the effort low thanks to the model's ability to delineate avalanches. The human corrections to the segmentation in the form of positive clicks on the avalanche or negative clicks on the background result in avalanche outlines of good quality with little effort. Relying on IAS, we extract avalanches from the images in a flexible and efficient manner, resulting in a 90% time saving compared to conventional manual mapping. The images can be georeferenced with a mono-photogrammetry tool, allowing for exact geolocation of the avalanche outlines and subsequent use in geographical information systems (GIS). If a webcam mounted in a stable position, the georeferencing can be re-used for all subsequent images. In this way all avalanches mapped in images from a webcam can be imported into a designated database, making them available for the relevant safety-related applications. For imagery, we rely on current and archive data from webcams that cover the Dischma valley near Davos, Switzerland and capture an image every 30 minutes during daytime since the winter 2019. Our model and the associated mapping pipeline represent an important step forward towards continuous and precise avalanche documentation, complementing existing databases and thereby providing a better base for safety-critical decisions and planning in avalanche-prone mountain regions.

1 Introduction

Information on avalanche occurrences is crucial for many safety-related applications: For hazard mitigation, the dimensions of past avalanches are crucial for planning new and evaluating existing protection measures (e.g., Rudolf-Miklau et al., 2015). For the derivation of risk scenarios and the estimation of avalanche frequency, past events are an important piece of information as well (Bründl and Margreth, 2015). Mapped avalanches are also used to fine-tune and further develop numerical avalanche simulation software like SAMOS or RAMMS (Sampl and Zwinger, 2004; Christen et al., 2010). Today information on occurred avalanches is still mainly reported and collected at isolated locations, unsystematically by observers and (local) avalanche warning services, though more recent research has proposed using satellite imagery (e.g., Eckerstorfer et al., 2016; Wesselink et al., 2017; Bianchi et al., 2021; Hafner et al., 2022). Depending on the source, these reports contain information on the avalanche type, the avalanche size, the approximate release time, the complete outlines or at least the approximate location, the aspect, the type of trigger as well as additional parameters. To enlarge the knowledge about avalanche occurrences, we propose a systematic recording of avalanches from webcam imagery. This usage of existing infrastructure allows for a large-scale application anywhere avalanche-prone slopes are already captured by webcams. Images can be acquired as frequent as needed without additional cost, enabling a near-realtime determination of release time. Furthermore, the sequence of images increases the chance of obtaining an image without low cloud cover or fog that would prevent avalanche documentation of the whole avalanche. Except for our own initial proposition (Hafner et al., 2023) and Fox et al. (2023), we do not know of any attempt that makes use of this data source for avalanche identification and documentation. Fox et al. (2023) proposed two models in their initial experimental study for automatic avalanche detection from ground-based photographs: one for classifying images with and without avalanche occurrences and the other for segmenting the contained avalanches with bounding boxes. In opposition to their focus on finding the images and areas containing avalanches, we are aiming at extracting the exact avalanche outlines from the imagery.

Detecting individual objects and determining their outlines is the objective of instance segmentation. This is important for example in the fields of autonomous driving (e.g., De Brabandere et al., 2017), remote sensing (e.g., Liu et al., 2022) and medical imaging (e.g., Chen et al., 2020). Numerous instance segmentation models have been proposed in recent years that are based on the superior image understanding capabilities of deep learning. Besides the quest for fully automatic methods, there is also an area of research dedicated to Interactive Object Segmentation (IOS), where a human collaborates with the computer vision model to segment the desired object with high accuracy but low effort (Boykov and Jolly, 2001; Gulshan et al., 2010; Xu et al., 2016; Sofiiuk et al., 2020; Kontogianni et al., 2020; Lin et al., 2022; Kirillov et al., 2023). The human operator explicitly controls the segmentation, first by an initial input to mark the desired object (e.g., through a click or scribbles), and then by iteratively adding annotations to correct the segmentation where the automatic model makes mistakes, gradually refining the result. The goal is an accurate segmentation, provided by the IOS model with as little user input as possible. The key difference to instance segmentation are the user corrections and the way they are processed and encoded in the model. The vast majority of models proposed in recent years are employing clicks from the user for correcting the segmentation (e.g., Boykov and Jolly, 2001; Rother et al., 2004; Xu et al., 2016; Benenson et al., 2019; Kontogianni et al., 2020; Sofiiuk et al., 2021) and are using

a combination of random sampling and simulating user clicks for training the model. The neighborhood of the clicked pixel is expanded to discs of three to five pixel radius or to Gaussians, depending on the model. When discs are used to encode clicks, the whole area specified by the radius is given the same weight. When clicks are encoded as Gaussians the weight is a Gaussian distribution, decreasing from the center of the click over the area specified by the radius.

There is only little work on webcam (-like) imagery, the dominant data source for automatic avalanche documentation so far has been satellite imagery (e.g., Bühler et al., 2019; Eckerstorfer et al., 2019; Hafner et al., 2021; Bianchi et al., 2021; Karas et al., 2022; Kapper et al., 2023). Optical satellite data, proven to be suitable to reliably capture avalanches (spatial resolution approx. 2m, or finer; Hafner et al., 2021, 2023), needs to be ordered and captured upon request which is expensive and dependent on cloud free weather conditions. Radar data has the big advantage of being weather independent, but with one satellite in operation, open access Sentinel-1 data is only available at selected dates (currently approx. every 12 days in Switzerland) and other suitable radar data needs to be ordered and purchased as well. Additionally, with a spatial resolution of approximately 10–15 m, it is not possible to confidently map avalanches of size 3 and smaller from Sentinel-1 imagery (Hafner et al., 2021; Keskinen et al., 2022). Furthermore, the exact or even approximate time of avalanche release cannot be retrieved from satellite data and remains unknown. However, where suitable satellite data is available, areas affected by avalanches may be identified and documented continuously over large regions with identical methodology.

Applications relying on information about avalanche occurrences not only seek confirmation of an avalanche near a specific webcam, but also require details such as the precise location, extent, aspect of the release area, and size of the avalanche. Avalanches captured on oblique photographs may be georeferenced to enable a transfer of the avalanche identified in the image to a map. There are several monophotogrammetry tools available to georeference single images, initially developed to georeference historic photographs (e.g., Bozzini et al., 2012, 2013; Produit et al., 2016; Golparvar and Wang, 2021). Only with existing georeferencing, the detected avalanches can be exactly geolocated, compared by size, aspect or slope angle as well as imported into existing long-term databases. Since most webcams are mounted in a stable position, always capturing the same area, the georeferencing only needs to be done once and may be re-used for all subsequent images.

To complement the currently established ways avalanche occurrences are documented, we propose to use webcam infrastructure regularly acquiring imagery for avalanche mapping. In the present work, we identify avalanches in imagery employing interactive object segmentation (Interactive Avalanche Segmentation, IAS). Since human user interactions are modeled during training we investigate the transferability of our model results to the real-world use by humans in a user study. We use webcam imagery from stations maintained by the WSL-Institute for Snow and Avalanche Research SLF (SLF) available every 30 minutes, in near-real time and the avalanche library published by Fox et al. (2023). Additionally, we propose a workflow to georeference the identified avalanches with the monophotogrammetry tool from Bozzini et al. (2012, 2013). By mapping avalanches from webcam imagery we enlarge existing avalanche databases, thereby allowing for better decision making for downstream applications.

2 Data

2.1 SLF Webcam network

Our webcam network covers the Dischma Valley, a high alpine side valley of Davos, with fourteen cameras mounted at six different locations (Fig. 1). The valley is about 13 km long, the valley floor reaches from 1500 m a.s.l to 2000 m a.s.l, while the summits reach heights over 3000 m a.s.l. The Dischma valley is permanently inhabited in the lower five kilometers while the road leading to its upper part is closed in winter. Steep mountains are located on both sides of the valley over and 80% of the entire area are potential avalanche terrain (Bühler et al., 2022). Outside the permanent settlements, avalanches can only be monitored remotely, especially during high avalanche danger.

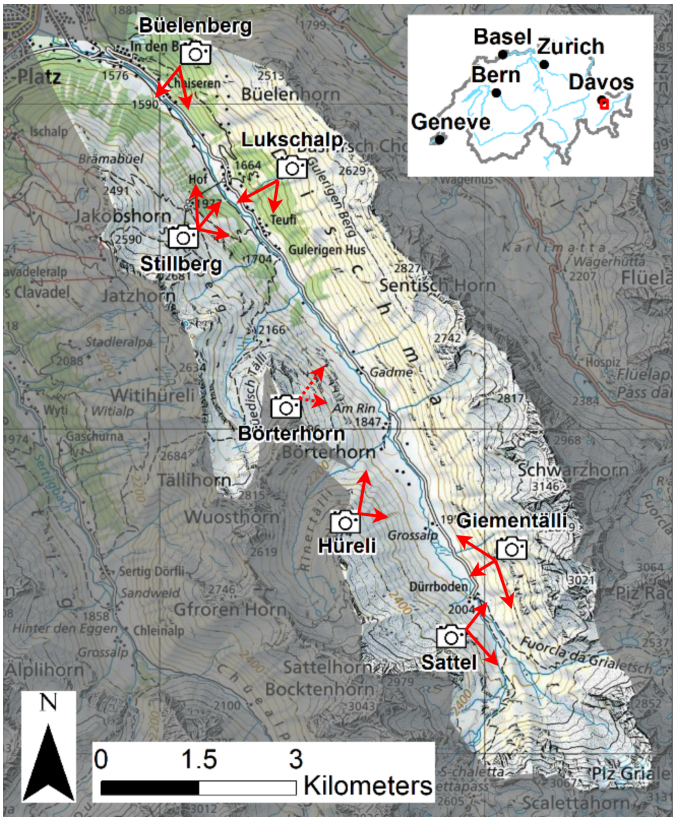

Figure 1. Locations, view directions (red arrows) and area covered by the fourteen cameras mounted in six different locations in the Dischma Valley, Davos. The Hüreli station succeeded the Börterhorn station (dashed arrows) which is no longer in operation (map source: Federal Office of Topography).

Each of our six stations is equipped with two to three cameras (usually a Canon EOS M100), operated with an independent power supply with a solar panel and a battery, except for Stillberg where we connected to existing power lines (Fig. 2). The acquisition of images every 30 minutes during daylight is programmed and automatically triggered by a small on-station-

computer. This interval lowers the risk of cloud cover, and captures avalanches under different illumination conditions, once they have occurred. The images are then sent to SLF in near-real time via the mobile network and stored on a server. The first camera was mounted at the Büelenberg station in summer 2019, with the next four stations being established in the following months. The Börterhorn station came later, has only been in operation from December 2021 to June 2023 and has been moved to a new location with similar view in December 2023 (Hüreli station). The images have previously been used in the ESA DeFROST Project (ESA, 2020) and in Baumer et al. (2023) .

(a) Station with two cameras, bolted to a rock face at Lukschalp.

(b) Station with (initially) three cameras, mounted on a mast at Sattel.

Figure 2. The stations in the Dischma valley were either mounted on a mast or bolted to rock faces. They host two to three cameras and all infrastructure necessary to ensure power supply as well as data acquisition and transmission.

2.2 Avalanche images and annotations

We used unique sets of images for the model to learn from (training), for the unbiased evaluation during training and hyperparameter tuning (validation) as well as for the unbiased evaluation of the final model (testing).

SLF dataset

We rely on imagery from the webcams at our stations for training (all except Börterhorn and Hüreli; Sect. 2.1), validation and testing. The images with a size of 6000×4000 pixels are from seven different cameras that captured well identifiable

avalanches since being in operation. For training, we prepared the images and cropped to 1000×1000 pixels, keeping only the avalanches and their immediate surrounding in the original resolution. For evaluating and for our user study, we want to segment all captured avalanches per image, therefore we only resized the images to 3600×2400, the largest the model may handle.

The avalanches in the images were manually annotated with the smart labeling interface provided by Supervisely (Supervisely, 2023). The *SLF dataset* contains roughly 400 annotated avalanches (Tab. 1). About three quarters are used for training, testing and validation, while the rest is used to test generalizability. For this, we use images with a certain domain gap relative to the training images: 46 images from the two Börterhorn webcams, excluded from training (*WebNew*) and a set of 44 images taken from handheld cameras (*GroundPic*; Tab. 1). The *WebNew* contains mostly small avalanches, some of them captured under diffuse illumination conditions, while the *GroundPic* depicts larger avalanches and includes some images of lower quality taken with mobile phones. For our user study, we relied on a combination of different webcam images showing avalanches of different sizes and captured under varying illumination conditions. Of the 20 annotated avalanches (*UserPic*), 75% are unique to the dataset, while the rest are also part of the *WebNew* or the *GroundPic*.

Table 1. Overview of the datasets used.

Dataset name	Avalanche annotations		Description
SLF	*train*	200	Webcam imagery and annotations from our test site in Dischma (Fig. 1).
	vali	44	
	test	45	
	WebNew	46	Imagery and annotations from the Börterhorn station (Fig. 1), whose two webcams were excluded from the *SLF train*, *vali* and *test* and have an unseen viewpoint relative to these images.
	GroundPic	45	Imagery and annotations taken from handheld cameras with an unseen viewpoint relative to all training images.
	UserPic	20	Imagery from webcams and corresponding annotations. 75% of the images are unique to this dataset while the rest are also part of the *WebNew* or *GroundPic*.
UIBK	*train*	2102	Imagery and annotations used by Fox et al. (2023, University of Innsbruck et al. (2023)).
	vali	382	
	test	867	

UIBK dataset

Fox et al. (2023) have published a dataset containing images of over 3000 avalanches from different perspectives with annotations of the avalanche type (slab, loose snow and glide snow avalanches; University of Innsbruck et al., 2023). In addition to avalanches, their category "glide snow avalanche" also contains glide snow cracks where no avalanche has occurred (yet).

We decided to include a selection of their annotations in some of our training configurations to evaluate the performance of our setup using a multi-source dataset. We are however interested in avalanches only, therefore we manually sorted out images with glide snow cracks and excluded them for training. Consequently, we used a subset of 2102 binary avalanche masks from the *UIBK dataset* for training and 382 avalanches for validation, which we prepared by cropping to 1000×1000 pixels (Tab. 1). For the test dataset, we kept all images, depicting 867 avalanches and glide snow cracks, to allow for a fair comparison to Fox et al. (2023). Fox et al. (2023) provide no details about the manual annotation procedure. We note that upon comparison, their annotations are markedly coarser than ours, with significantly smoother and more generalized avalanche outlines (e.g., Fig. 3). We resized the images larger than 3600×2400 to that size for the evaluation.

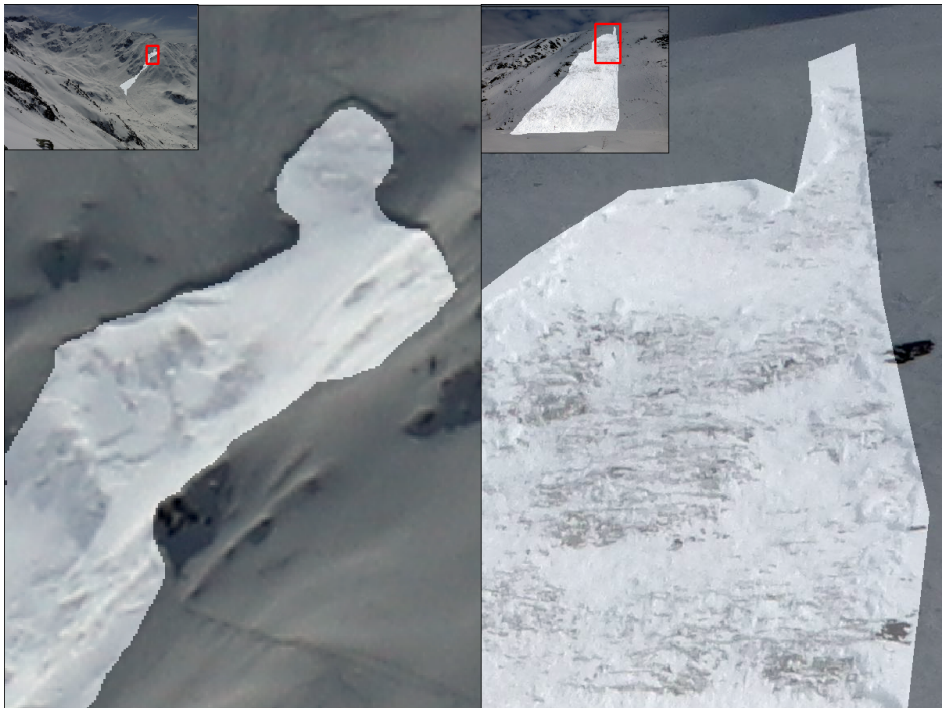

Figure 3. Comparing the details in the annotation from one of the *SLF* webcam images (left) to an image from the *UIBK dataset* (right; University of Innsbruck et al. (2023)).

3 Methodology

We used a state-of-the-art interactive image segmentation model (Sofiiuk et al., 2021), modified it for avalanches, and trained it with three different sets of avalanche imagery. The trained model was then applied to new, unseen images to qualitatively and quantitatively evaluate the resulting avalanche outlines using both per-pixel and per-avalanche metrics. It is important to note that click locations have to be selected automatically to enable large-scale training and testing. This could lead to performance

differences caused by deviations between simulated clicks and real user behaviour. We therefore additionally designed and carried out a user study with human annotators to ascertain that the efficiency gains carry over to the real use case.

3.1 Model architecture

We employed the interactive segmentation model introduced by Sofiiuk et al. (2021), adapted it specifically to avalanches and trained it with a variety of avalanche datasets. Sofiiuk et al. (2021) used the HRNet+OCR method, a High-Resolution Network (HRNet) with an added Object-Contextual Representations module (OCR; Wang et al., 2020; Yuan et al., 2020; Xu and Zhao, 2024). The HRNet+OCR architecture connects high- and low-resolution convolutional processing streams in parallel and enables information exchange across different resolutions (Wang et al., 2020). The OCR module explicitly accounts for global context to achieve better segmentation of objects in complex images (Xu and Zhao, 2024), which is particularly valuable in our case of avalanches that can make up large parts of the images while being hard to distinguish from the white snow in the background if considering only local evidence. Positive and negative click locations from interactive user input were encoded as discs with a fixed radius of 5 pixels (Benenson et al., 2019).

Semantic segmentation backbones usually take only RGB images as input, for interactive segmentation, the handling of additional model input, in our case encoded user clicks, needs to be carefully implemented (Fig. 4). Sofiiuk et al. (2021)'s solution to this is Conv1S: a convolutional block that outputs a tensor of exactly the same shape as the first convolutional block in the backbone. The output of the first backbone convolutional layer (usually 64 channels) is then summed up element-wise with the convolutional block applied to the encoded user clicks. With this implementation, it is possible to choose a different learning rate for new weights without affecting the weights of a pre-trained backbone.

A combination of random and iterative sampling strategies are employed to simulate human user clicks for training, with masks from previous steps included in the iterative sampling procedure (Fig. 5). Morphological erosion is used to shrink the largest mislabeled region before setting the sampling point into its center, which proved to be superior to simply setting the next click in the center of the erroneous region (Mahadevan et al., 2018). The click may be positive, denoting the avalanche, or negative for the background. In the evaluation mode, the click is put at the center of the largest erroneous region, be it false positive or false negative, as proposed in Xu et al. (2016) or Li et al. (2018). The maximum number of clicks (positive or negative) is set to 20 for both training and evaluation.

We made the following adaptions to the original model from Sofiiuk et al. (2021):

- we trained on patches of 600×600 pixels instead of 320×480, that we cropped from varying places of our training images
- for data augmentation during training, we additionally included random translation (max. 3%) and rotation (max. 10 degrees)
- we replaced the manual multistep learning rate scheduler by a cosine learning rate scheduler to profit from a a decreasing learning rate without the need to fiddle with the steps and rates of decay

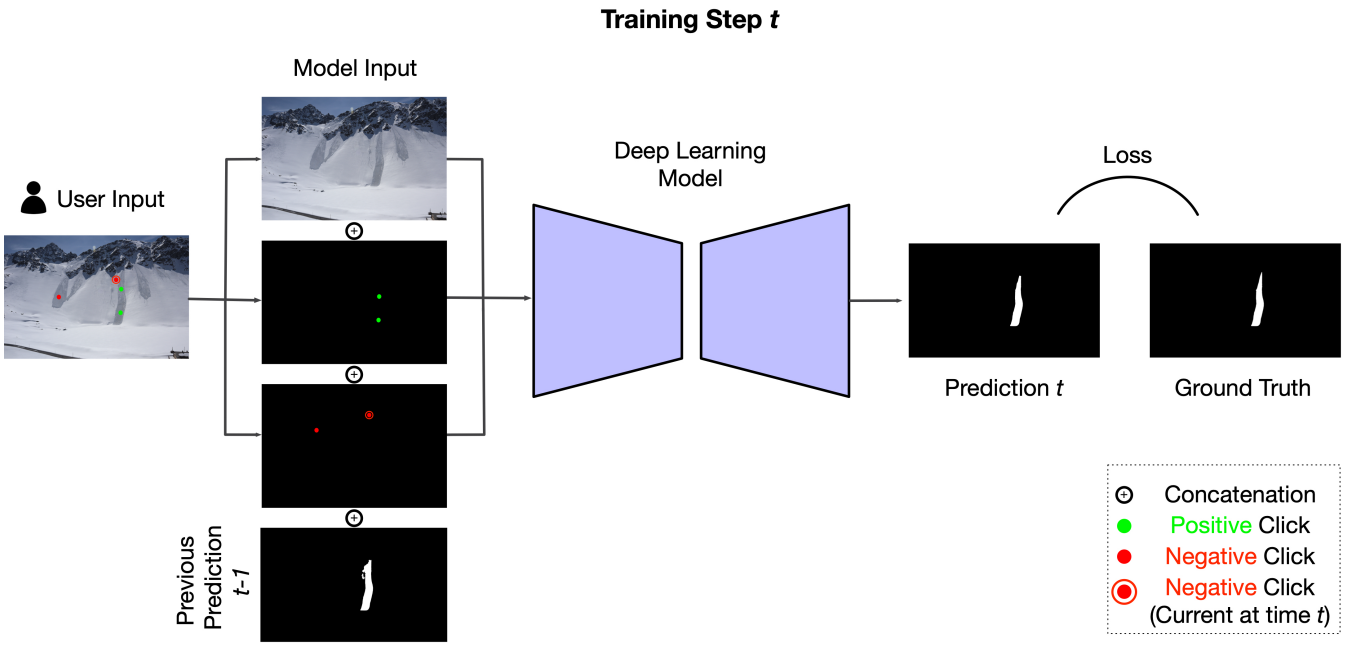

Figure 4. Illustration of the finetuning step of the IOS when training on avalanches.

- we did not use the zoom-in function
- we used a batch size of 4 instead of 28 due to our relatively small training dataset but fine image resolution

3.2 Evaluation metrics

The raw predictions (i.e., the per-pixel probabilities for being part of the avalanche) were thresholded at 0.5 to obtain binary avalanche masks for the analyses. We used the Intersection over Union (IoU) as an indicator of spatial agreement between either the predicted and ground truth masks or the bounding boxes around those masks (e.g., Levandowsky and Winter, 1971).

Pixel-wise metrics

On the pixel level of the masks, we recorded the average Number of Clicks (NoC) necessary to reach IoU thresholds of 0.8 and 0.9, respectively (denoted as mNoC@80 and mNoC@90). Achieving a high IoU after few clicks makes the model most useful. Consequently, we compared the IoU at click k (for k = 1,2,....,20) averaged over all the images (mIoU@k). Additionally, we calculated the number of images that do not reach 0.85 IoU, even after 20 clicks (NoC_{20}@85).

Object-wise metrics

On the object-level, we compared the IoU of the bounding box of the predicted and the ground truth avalanche annotation. If the IoU between two bounding boxes is larger or equal to a threshold T, the detection is considered correct, while for values below the threshold T it is not (Padilla et al., 2020). Like Fox et al. (2023), we first considered a T $\geq$ 5% between the bounding

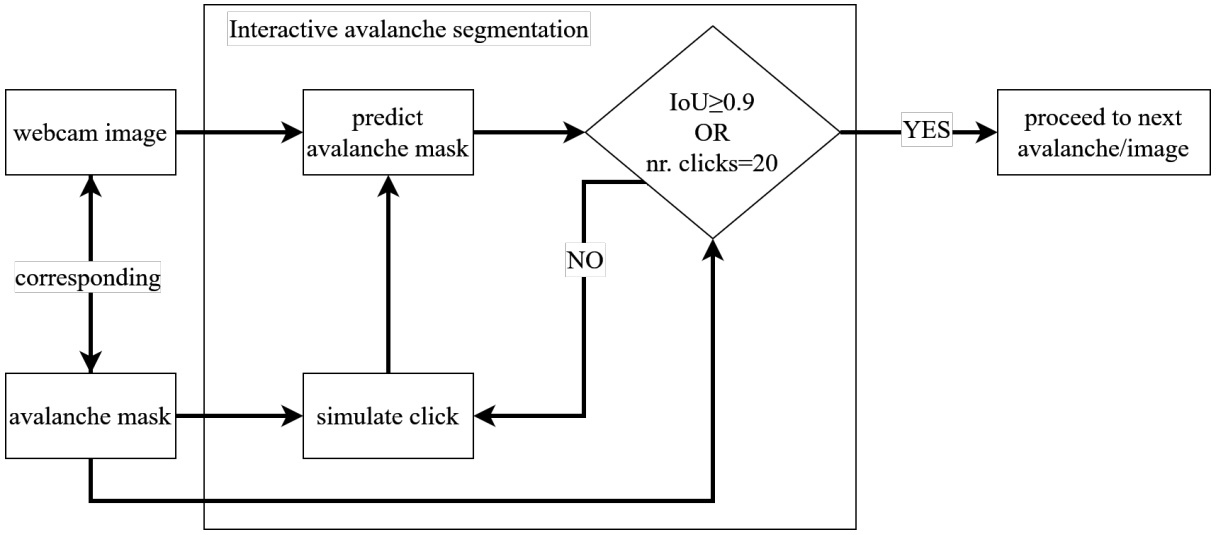

Figure 5. Illustration on the handling of one avalanche when training the IAS model with clicks generated by random and iterative sampling. For the new prediction all previous clicks, as well as the previous mask (if available) are considered.

boxes as a match, but additionally we evaluated with T $\geq$ 50%, which is more standard value in literature (Redmon et al., 2016; He et al., 2018).

From the matches, we computed the F1-score as

$$\mathrm{F1} = 2 \cdot \frac{\mathrm{PPV} \cdot \mathrm{POD}}{\mathrm{PPV} + \mathrm{POD}}, \tag{1}$$

where Probability of Detection (POD) and Positive Predictive Value (PPV) are defined as

$$\mathrm{POD} = \frac{\mathrm{TP}}{\mathrm{TP} + \mathrm{FN}} \qquad \text{and} \qquad \mathrm{PPV} = \frac{\mathrm{TP}}{\mathrm{TP} + \mathrm{FP}}, \tag{2}$$

where TP is true positive, FP is false positive and FN is false negative.

Comparison of time needed

The time spent to map an avalanche with the "traditional method", like the avalanches part of the DAvalMap inventory (Hafner et al., 2021), is not recorded by default. For a comparison to the time spent on IAS, we had one experienced person record the number of minutes needed for manually mapping 274 avalanches from photographs (mean size 1.75; European avalanche size definition (EAWS, 2023)), with the methodology described in Hafner et al. (study 2; 2023).

3.3 Experimental setup

To find the best model for interactively segmenting avalanches from our webcam imagery, we evaluated several training regimes, all with the same model architecture but varying training datasets (see Sect. 3.1). Our baseline was the model trained only on *COCO+LVIS* (104k images and 1.6M instance-level masks; Lin et al., 2015; Gupta et al., 2019), meaning that it has

never seen an avalanche. We then trained three further versions, re-using the already learned knowledge from being trained on *COCO+LVIS*, and fine-tuning the model with different sets of avalanche data: AvaWeb trained on the *SLF dataset*, AvaPic trained on the *UIBK dataset* and AvaMix trained on a combination of those two (Tab. 1). Preliminary tests confirmed that fine-tuning the model pre-trained on *COCO+LVIS* was always superior to training from scratch using only avalanche data. This is in line with previous work on avalanches (Hafner et al., 2022). We performed hyperparameter tuning on the validation set (e.g. selecting the ideal number of training epochs: 90 for AvaWeb and AvaPic, 95 for AvaMix and using a threshold of 0.5 on the raw predictions). We used the hyperparameters selected on the validation set fixed during our evaluation on the test set. For evaluation, we checked how well the model generalizes to the *SLF test* as well as to images from other webcams (*WebNew*). We additionally evaluated the *GroundPic* and the *UIBK test* to assess the robustness of the model configurations to images from outside our webcam perspective. In addition, we compared to segmentation results from previous work by Fox et al. (2023), by calculating bounding boxes for our predictions and evaluating their overlap with respect to the ground truth bounding boxes from the *UIBK test*.

3.4 User study

We carried out a small user study, to investigate if the metrics from evaluating our model hold with real users whose input is noisier and who may adapt to model behaviour. Eight participants were given a short introduction and mapped one avalanche per *UserPic* image. For our user study, we used the GUI provided by Sofiiuk et al. (2021), adapting it to save the click coordinates, the time needed per click, as well as the predicted masks for each click together with the IoU. Since several images captured more than one avalanche, we added an arrow pointing at the desired avalanche in each *UserPic* image. Before segmenting the marked avalanches in *UserPic*, the participants performed two trial segmentations that were not used for evaluation, to familiarize themselves with the GUI, the annotation protocol and the data characteristics. Participants were allowed a maximum number of 20 clicks per avalanche, but were told they could stop earlier if they were satisfied with the segmentation. As metrics for the user study, we calculated the mNoC@80 and mNoC@90, compared the mIoU@k, the mean annotation time, the NoC_{20}@85, as well as the differences between the best and worst results in terms of mean IoU. To investigate variability in the avalanche areas identified, like in Hafner et al. (2023), we calculated pairwise IoU scores for the final masks from the last employed click per participant. To test whether the differences between the mIoU scores of the participants are statistically significant, we used the two-sided t-test (as implemented in R Core Team, 2021) with significance level $p \leq 0.05$.

4 Results

Pixel-wise metrics

Evaluating on the *SLF test* the model trained on the AvaWeb was almost 10% better than the others and almost 25% better than the baseline (*COCO+LVIS*; Fig. 6) from click 1. It remained on top but the others caught up by approximately click 16. AvaPic was consistently the worst at high click numbers and even dropped below the baseline. Adding the data from AvaWeb

to AvaPic in the AvaMix improved the results, but only got about halfway to the AvaWeb alone. Compared to the baseline, all models trained with avalanches were superior to the baseline, especially for the first half of the clicks and except for the AvaPic for the last half of the clicks. Overall, the AvaWeb needed the least clicks for reaching the desired IoU thresholds and only for one image never reached the NoC_{20}@85. The AvaPic, never reached this threshold for five images while this was the case for only two images for the AvaMix and even the baseline reached an IoU of 85% for more images. For the remaining analyses, we did not consider the model trained only on *COCO+LVIS* (baseline).

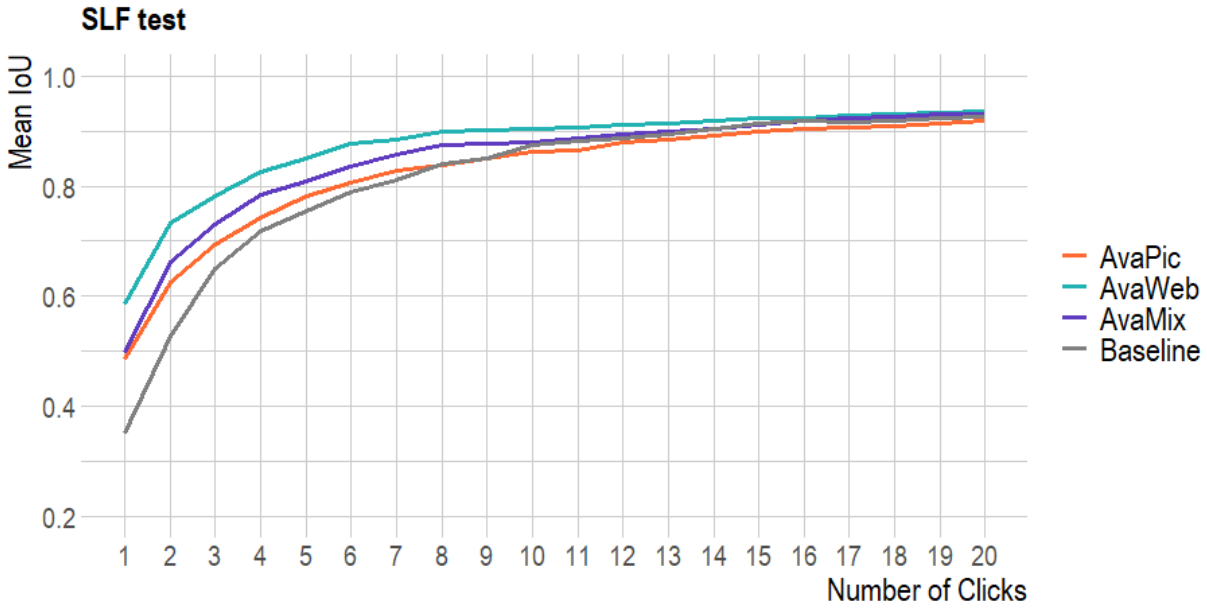

Figure 6. Evaluation on the *SLF test* based on models trained with different datasets: Baseline (*COCO-LVIS*), AvaWeb (*SLF train*), AvaPic (*UIBK train*) and AvaMix (*SLF + UIBK train*).

Table 2. Results for the different datasets when evaluating on the *SLF test*.

Model	Pretrained weights	mIoU@1 [%]	mIoU@2 [%]	mIoU@3 [%]	mNoC@80	mNoC@90	NoC_{20}@85
COCO+LVIS (baseline)	-	35.07	52.62	65.00	5.58	9.42	3
AvaWeb	*COCO+LVIS*	**58.59**	**73.40**	**78.30**	**3.31**	**7.6**	**1**
AvaPic	*COCO+LVIS*	48.50	62.51	69.42	5.24	10.73	5
AvaMix	*COCO+LVIS*	49.75	66.24	73.03	4.11	9.4	2

To check how well the models generalize to new avalanches under varying perspectives, we evaluated them on the *WebNew*, the *GroundPic* and the *UIBK test* (Fig. 8, Tab. 3): AvaWeb was superior with a margin of up to 30% from click 1 over the

AvaPic and AvaMix on the *WebNew* (Tab. 2; Fig. 7). The AvaPic and AvaMix only caught up around click 10, but never surpassed the AvaWeb. For all models, the images in the $NoC_{20}@85$ category depicted small, often long and slim avalanches located in the shade, on imagery acquired under diffuse illumination conditions and/or avalanches that had been snowed on, reducing overall visibility of the features (Fig. 9).

Figure 7. Example for an image from the *SLF test* that all three models solved well. The lighter the hue in the model predictions the higher the model certainty concerning the existence of an avalanche. In a close-up look the AvaWeb prediction exhibits more nuanced and detailed avalanche boundaries.

On the ground-based *GroundPic*, the AvaWeb started out being the worst by a margin of about 10%, while it caught up and surpassed the AvaPic from click 5 onwards but never reached the AvaMix. For the large but more coarsely annotated *UIBK test*, the AvaPic and the AvaMix were consistently superior to the AvaWeb by 10 to 20%. The AvaWeb struggled the most with ground-based close-up views of avalanches, often in combination with diffuse illumination conditions or shade as well as avalanches captured on coarse images from mobile phones (Fig. 10). For some of those avalanches, the IoU score reached after 20 clicks is well below 50%. For more than one quarter of all avalanches, the AvaWeb never reached the $NoC_{20}@85$, while for the AvaPic and AvaMix less than 1% of all avalanches never reached an IoU of 85%. The AvaPic and AvaMix struggled mostly with the same images, which depicted close-up views of the release area of avalanches in diffuse illumination conditions or avalanches which have been snowed on and are hard to spot.

Object-wise metrics

Comparing bounding boxes, the AvaWeb achieved an F1 score 0.12 higher than Fox et al. (2023), from the first click onwards (0.64 vs. 0.76; bounding box threshold 0.05; Tab. 4). For both the AvaPic and the AvaMix, the F1 score was even close to 1, therefor by 0.33 to 0.34 superior to Fox et al. (2023) and higher than the AvaWeb. With a threshold of 0.5 for the overlap of the bounding boxes, the scores were lower and lay between 0.23 (AvaWeb) and 0.44 (AvaPic) for the first click. Consequently, the AvaPic and the AvaMix were again superior to the AvaWeb (by around 0.2) and remained on top for click 3 and 5 also. For click 5, the AvaPic and the AvaMix already achieved an exceptionally good F1 score above or equal to 0.94. No comparison to Fox et al. (2023) was possible for the 0.5 bounding box threshold.

User study and time saved

For our user study, we loaded the model trained on AvaWeb for making predictions upon user input. On average, the participants employed 4.9 clicks for the *UserPic*, with variations from 1.25 to 9.63 clicks for the 20 different images. The employed clicks were on avalanches in 79% of all cases, while the rest was on the background. The avalanches that needed fewer clicks to

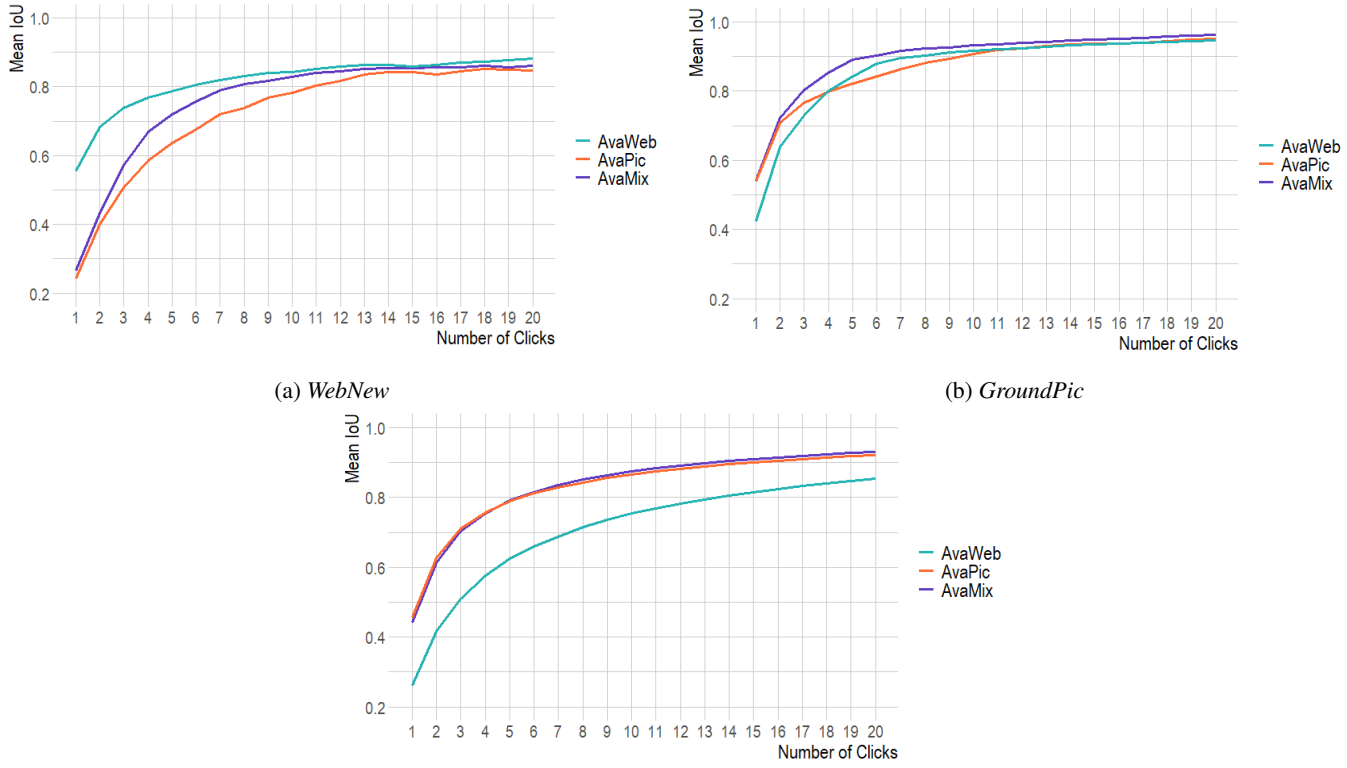

(a) *WebNew*

(b) *GroundPic*

(c) *UIBK test*.

Figure 8. Comparing mIoU per click for three datasets with a domain gap to the initial webcam data for our three training configurations: AvaWeb (*SLF train*), AvaPic (*UIBK train*) and AvaMix (*SLF + UIBK train*).

Table 3. Results when evaluating the generalizability on data not seen during training with a domain gap with respect to the training data.

Dataset	Model	mIoU@1 [%]	mIoU@2 [%]	mIoU@3 [%]	mNoC@80	mNoC@90	NoC_{20}@85
WebNew	AvaWeb	**55.61**	**68.24**	**73.85**	**6.65**	**13.57**	**12**
	AvaPic	24.31	40.08	50.76	10.78	16.07	15
	AvaMix	26.72	43.26	57.20	9.07	14.39	14
GroundTest	AvaWeb	43.32	63.43	73.38	4.53	**6.91**	2
	AvaPic	54.63	71.25	76.92	3.98	7.73	2
	AvaMix	**54.82**	**72.72**	**80.51**	**3.09**	6.96	**1**
UIBK test	AvaWeb	26.19	41.71	51.05	10.47	15.82	246
	AvaPic	44.28	61.29	70.37	**5.84**	**11.26**	**50**
	AvaMix	**45.70**	**62.67**	**70.99**	6.06	11.72	75

Figure 9. Example for an image from the *WebNew* with diffuse illumination and a long and slim avalanche that all three models struggled with. The lighter the hue in the model predictions the higher the model certainty concerning the existence of an avalanche.

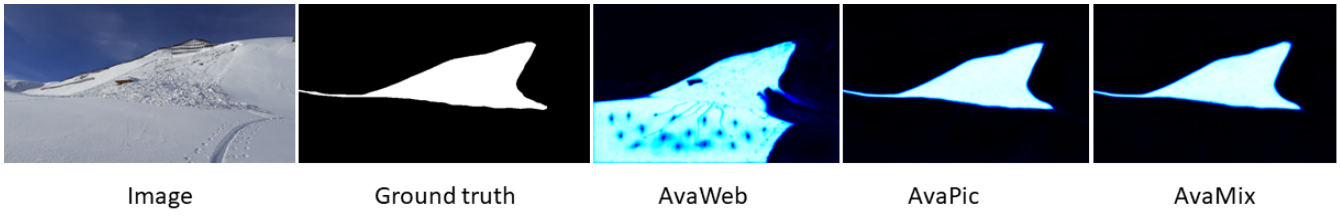

Figure 10. Example of a close-up view of an avalanche from the *GroundPic*, where the AvaWeb struggled with correctly identifying the avalanche area close to the photographer. The lighter the hue in the model predictions the higher the model certainty concerning the existence of an avalanche.

reach a certain IoU threshold tended to be the smaller ones. Even though not everyone always clicked until an IoU of 85% was reached, on average only one image remained below that value. This image depicted an avalanche that is located in a partly shaded and partly illuminated area, where especially in the shade features are hard to identify. On average participants needed 6.5 seconds to reach an IoU of 80% and 9.1 seconds for an IoU of 90%. In opposition, on average 2 minutes and 36 seconds were required for mapping one avalanche with the "traditional method", with time needed ranging from one to eight minutes. This is more than 2 minutes extra than when relying on IAS and translates to greater than 90% saving in time compared to a manual mapping.

In our user study, we observed large variations between the different participants: for the average number of clicks (2.90 to 8.10), the mNoC@80 (1.80 to 2.80) and the mNoC@90 (2.00 to 3.12). Additionally, for avalanches like in Fig. 11 (top) there was no clear "middle" to place the first click which resulted in very diverse click strategies for the participants. In contrast, for the avalanche in Fig. 11 (bottom) clicks were placed more homogeneous first in the "middle" and then at the top and bottom, thereby correcting details. For clicks 1 to 5, where we had enough samples from all participants, we checked if the differences between the highest and the lowest mIoU were statistically significant. The differences were not significant for IoU@1 and IoU@2 (t-test: p-value: > 0.05) but they were statistically significant for IoU@3 (p-value= 0.045), IoU@4 (p-value= 0.034) and IoU@5 (p-value= 0.035). This was caused by very consistent results with low standard deviation for the participants with the highest mIoU@k scores. When taking the mask from the last click as a final result, the differences between participants

Table 4. Comparison of F1 scores and standard deviation for the two different IoU thresholds (5% like Fox et al. (2023), and 50%) on the *UIBK test*.

F1 score ± std	**IoU 5%**				**IoU 50%**		
	Fox et al. (2023)	AvaWeb	AvaPic	AvaMix	AvaWeb	AvaPic	AvaMix
automated	0.64 ± 0.60	-	-	-	-	-	-
click 1	-	0.76 ± 0.43	**0.97** ± 0.16	0.96 ± 0.20	0.23 ± 0.42	0.44 ± 0.50	0.42 ± 0.49
click 3	-	0.99 ± 0.11	**1**	1 ± 0.05	0.66 ± 0.47	0.86 ± 0.34	0.87 ± 0.31
click 5	-	1 ± 0.08	**1**	**1**	0.80 ± 0.40	0.94 ± 0.24	0.96 ± 0.20

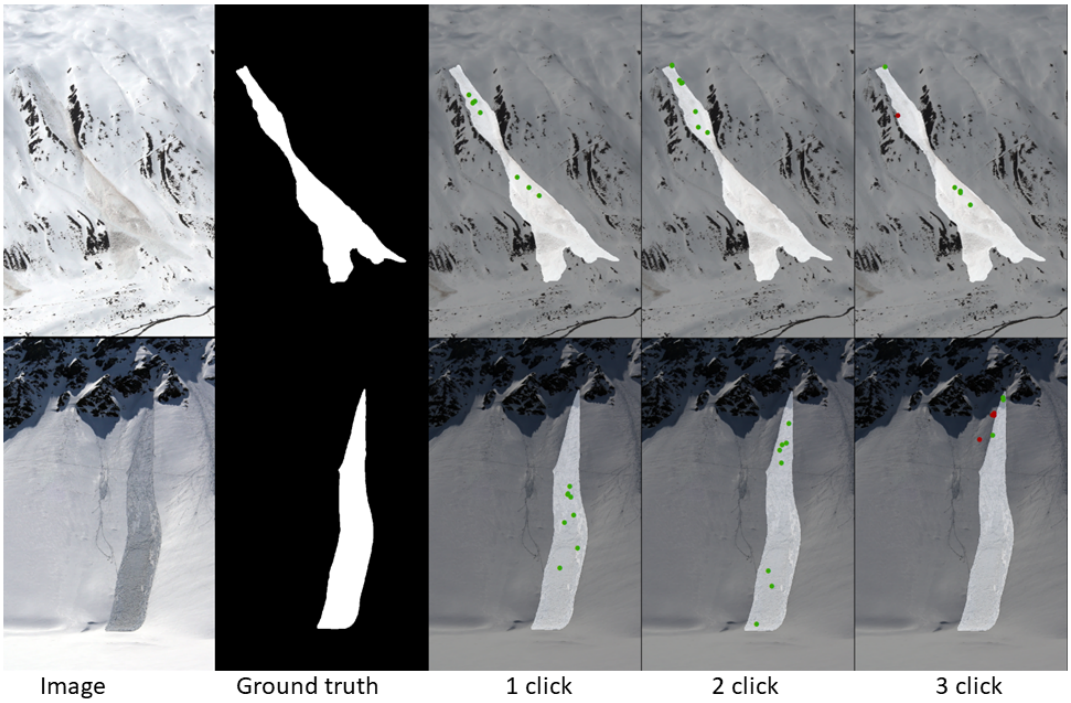

Figure 11. Illustration where the first three clicks in two images from the *UserPic* dataset were placed. Green dots denote positive clicks, red dots denote negative clicks.

were however quite small: the mean pairwise IoU was 93.53%, the maximum 95.44% and the minimum 90.59%. Consequently, all pairs had an IoU within 5% of each other as their segmented final avalanche masks were very similar (Fig. 13).

When evaluating teh model trained on AvaWeb on the *UserPic* with simulated clicks and comparing to the user study results (see Tab. 5), the AvaWeb results were superior for all investigated metrics, except the mNoC@80. The participants with the highest mIoU@k held up to the numbers from the model (Fig. 13).

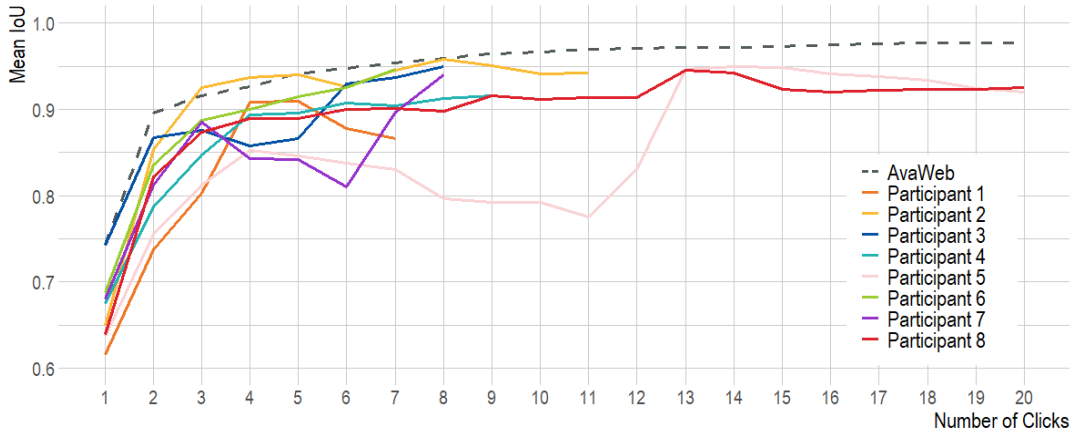

Figure 12. Comparison of the mIoU for all participants of the user study to the mIoU of the AvaWeb evaluated on the *UserPic* dataset. Note that only two participants used the maximum possible number of 20 clicks.

Table 5. Comparison of the results from the user study with the model results when evaluating on the same imagery (*UserPic*; N = 20).

	User Study	AvaWeb
mNoC@80	2.11	1.85
mNoC@90	2.50	2.55
NoC_{20}@85	1	0
mIoU@1 [%]	66.61	74.31
mIoU@2 [%]	80.91	89.57
mIoU@3 [%]	86.22	91.53

5 Discussion

Our results show that IAS enables segmentation of avalanches from webcam imagery within seconds. We compared the performance of the model trained with different datasets: As expected the model trained with any avalanche dataset outperformed the baseline (COCO+LVIS). The model trained on AvaWeb performed best for the two test datasets containing webcam imagery (*SLF test* and *WebNew*), performed on par with the dataset with a perspective unlike those of the webcams (*GroundPic*), but failed to generalize well to the large but coarsely annotated *UIBK test* with a large variety of perspectives and resolutions. In contrast, the model trained on larger and more diverse datasets (AvaPic and AvaMix), exhibited lower mIoU scores and a higher amount of clicks to reach a certain IoU for all test sets containing webcam imagery (*SLF test* and *WebNew*), but they performed better on imagery not from webcams (*GroundPic* and *UIBK test*). The model trained on AvaMix seems to have learned more details since the mIoU scores were higher than for the AvaPic for three out of four datasets from approximately click 3 to 10. During those clicks, after the initial coarse segmentation, details of the avalanche are segmented. We suspect that the detailed annotations, following the visible texture from the *SLF dataset*, helped the AvaMix to outperform the AvaPic.

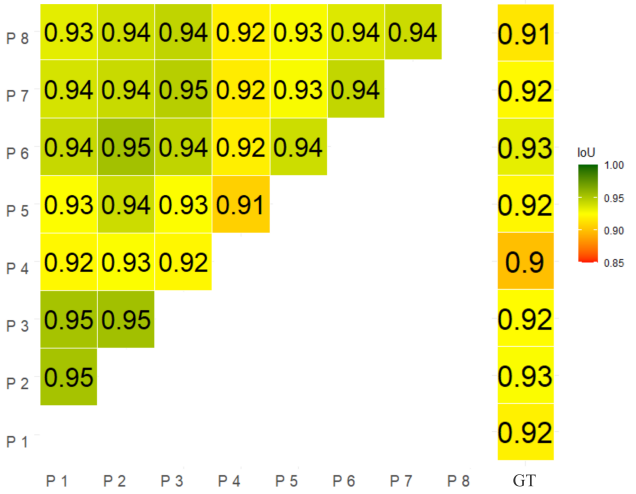

Figure 13. IoU for all participant pairs (Participants denoted as P, the ground truth as GT) for the final masks from our user study on the *UserPic*.

Overall, the model struggled with images of avalanches recorded under unfavorable illumination conditions. This is in line with previous studies that found the agreement between different experts for manual mapping to be lower in shaded areas (Hafner et al., 2022, 2023). Furthermore, especially the AvaWeb struggled with close-up views of avalanches, often these images are photographed from below the avalanche, resulting in a very specific perspective that the model has never seen during training. But overall, the AvaWeb, with less than 10% of the training data of the other two datasets, achieved the best performance for two out of three test sets with detailed avalanche annotations (*SLF test*, *WebNew*, *GroundPic*). Even though the *UIBK test* contained perspectives unknown to the AvaWeb, we believe the low performance, approximately 20% lower IoU, compared to AvaPic and AvaMix, is mostly caused by the coarseness of the annotations in combination with low resolution imagery, which the model struggles to reproduce. But results also showed that any model trained on avalanches is better than the baseline which has never before seen an avalanche. We believe the coarseness of the annotations in the AvaPic prevents the model from learning all it could from such a large and diverse dataset. Investigating this in more detail is beyond the scope of this paper but, future work should consider experimenting with a larger dataset of finely annotated avalanches covering various perspectives, avalanche types, avalanche sizes as well as snow and illumination conditions.

For their fully automated method, Fox et al. (2023) only evaluated bounding box overlap which is less challenging than the pixel overlap we focused on. When comparing our IAS best models bounding boxes on the first click to their results, we outperformed their F1 score by a large margin (0.64 vs. 0.97). Consequently, we captured the area that the avalanche covers better from the first prediction onwards.

In our user study, the participants with the best performance were as good as the simulation, but the mean IoU scores of all participants did not exceed the model (Tab. 5). We attribute this to the lack of serious training (visible in the variations of the number of clicks and time used) and knowing that estimations of avalanche area exhibit large variabilities (Hafner et al.,

2023) as there is no clear unambiguous definition of an avalanche boundary. Since the differences between the model and the participants were rather small, we consider the way user clicks are simulated during training representative of employed real-life click strategies.

Previous work (Hafner et al., 2023) found variations of up to 43% between experts when mapping avalanches from oblique photographs or from remote sensed imagery. In opposition to Hafner et al. (2023), our mean pairwise IoU scores for the avalanche area mapped (pixels in our case), were all within 5% of each other and all have an IoU above 0.9 with respect to the ground truth mask (Fig. 13). We believe having humans collaborate with the same underlying model homogenizes the avalanche area identified, as it guides the participants and constrains the results. Consequently, IAS not only improves efficiency but enhances the reliability, defined as the consistency of repeated measurements or judgements of the same event relying on the same process (Cronbach, 1947). Even though we had no overlapping avalanches in our *UserPic*, we still believe our findings also apply in this more challenging scenario.

As opposed to fully automatic avalanche segmentation IAS requires a human annotator. We do not see this as a disadvantage, but rather complementary since humans are present and will remain present in the future in many settings where avalanches are recorded, either connected to work or as part of winter leisure activities in the mountains. Compared to the traditional way of mapping avalanches, IAS saves over 90% time. We believe that the time saved may be even greater since the avalanches with a time recording were rather small (mean size 1.75; European avalanche size definition (EAWS, 2023)) compared to the ones in the user study and all located in an area well known to the person mapping. In practice, when using the tool to segment new avalanches, the user needs to decide when the predicted and corrected mask is detailed enough. Consequently, the final masks are the most important.

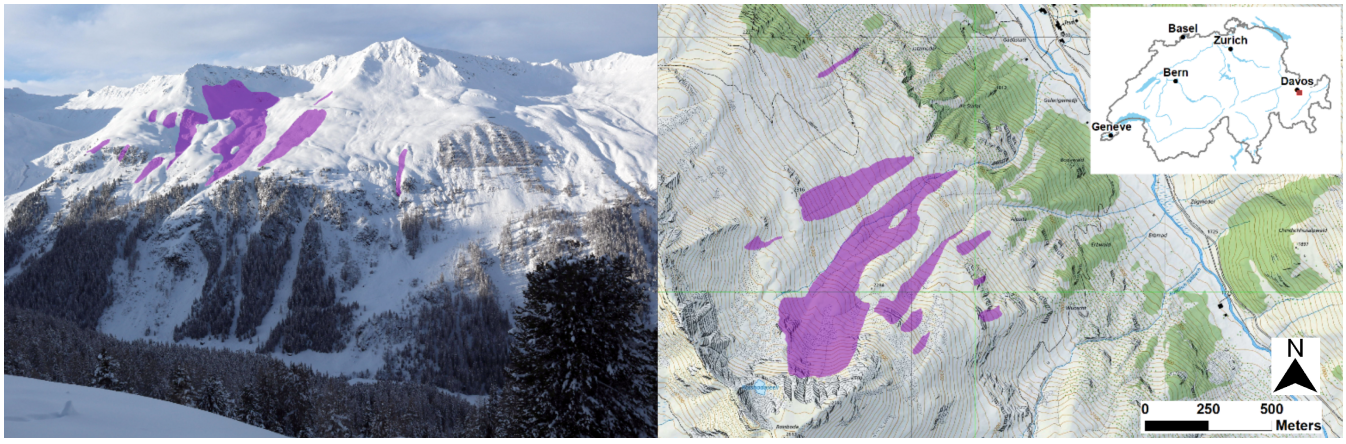

Figure 14. Example of avalanches segmented from an image with AvaWeb (left) and the corresponding avalanches displayed on a map after they have been georeferenced with the monoplotting tool (right, Bozzini et al. (2012); map source: Federal Office of Topography).

Webcams have limited coverage and cannot record avalanches in a spatially continuous manner like satellite imagery may (Bühler et al., 2019; Eckerstorfer et al., 2019; Hafner et al., 2022), but their temporal resolution is superior and allows

for a better monitoring of the avalanche activity over the course of the winter, leading to more complete datasets allowing for more detailed analysis of e.g. predisposition factors. The inclusion into existing databases however, requires the georeferencing of the avalanches, achievable with e.g. monophotogrammetry tools like Bozzini et al. (2012, 2013), Produit et al. (2016) or Golparvar and Wang (2021). The georeferencing allows for avalanches segmented in an image to be displayed on a map (like exemplary shown in Fig. 14). Without that, the application is limited to providing an overview on the current activity to an avalanche warning service, while all other downstream applications cannot profit from the data.

6 Conclusions and Outlook

We introduce a novel approach to map avalanches from webcam imagery employing Interactive Object Segmentation. During training the user's clicks that guide and correct the segmentation were simulated, optimizing the model to quickly identify the features of an avalanche. With IAS, a human user may, in seconds instead of minutes, segment the desired avalanche in collaboration with the model. Compared to satellite imagery, webcam imagery covers only limited areas. However, the abundance of webcams and possibility to acquire images as frequent as needed without additional cost, increases the likelihood of capturing avalanches even under adverse visibility conditions, offering a very valuable complementary data source for existing avalanche databases. This allows documentation of the avalanche activity for a whole season compared to just one extreme event like in Bühler et al. (2019). Additionally, the release time may be determined with less uncertainty, helping the avalanche warning and research to better connect the snow and weather conditions to avalanche releases.

In combination, IAS and georeferencing have great potential to improve avalanche mapping: Existing monophotogrammetry tools may be used to import avalanches detected with IAS from webcams. Assuming the camera position and area captured is stable, the georeferencing can be reused for all subsequent images. In the past this has been done for webcam-based snow cover monitoring (Portenier et al., 2020). In the future, existing approaches could be enhanced and expanded to a pipeline hosting the entire process from IAS to georeferencing and for importing the detected avalanches into existing databases. Furthermore, we see potential to automatically georeference images from mobile devices with the available information on the location and orientation in combination with the visible skyline and a digital elevation model (DEM). This would allow avalanche observers and the interested backcountry skiers to photograph an observed avalanche, quickly segment it with IAS and automatically send the georeferenced outlines to existing databases making them available to e.g. the avalanche warning service. This would make the outlines and geolocation of avalanches mapped in the field more reliable, compared to the "traditional" mapping approach described in Hafner et al. (2023). The possibility to record observed avalanches in an easy way could also help to motivate more people in reporting observed avalanches and therefore enlarge current databases with valuable detailed records.

Compared to the currently widely used mapping method (study 2; Hafner et al., 2023), segmenting an avalanche with IAS saves over 90% time and the results are more reliable in terms of consistency between mappings from different individuals. For the future we recommend training with a larger dataset with fine annotations and various perspectives, avalanche types, avalanche sizes as well as snow and illumination conditions. Our results indicate this would significantly help the model to segment fast and detailed as well as generalize well to all sorts of unseen perspectives. For fast image annotation or correcting

existing annotations with minimum user input our current model may be used. Annotations generated with IAS may, in addition, be used to develop and enhance models for automatic avalanche segmentation, saving time while generating outlines that follow the visible avalanche textures, easing the learning, thereby getting more accurate and reliable avalanche annotations in the future. Overall, this is a promising approach for continuous and precise avalanche documentation, complementing existing databases and thereby providing a better base for safety-critical decisions and planning in avalanche-prone mountain regions.

Code and data availability. The code will be made available upon publication of this paper together with the images and avalanche annotations.

Author contributions. EDH and TK came up with the initial idea, EDH coordinated the study, collected the images and annotated the avalanches used for training. EDH and LO adapted the model for avalanches and EDH did the analyses and organized the user study. TK, RCD, JDW and KS advised on the machine learning aspects of the project and critically reviewed the associated results. EDH wrote the initial manuscript and all co-authors critically reviewed and complemented it.

Competing interests. The authors declare they have no competing interests.

Financial support. The initial development and mounting of the majority of the webcams was part of the DeFROST project financed by the European Space Agency (ESA; N.4000127451/19/NL/CLP).

Acknowledgements. We thank the SLF Workshop and Electronics for developing, building and setting up our camera system in the Dischma valley. We are grateful to Simon Aeschbacher, Jor Fergus Dal, Amelie Fees, Julia Glaus, Matthias Lichtenegger, Isabelle Rittmeyer, Pia Ruttner-Jansen and Linda Zaugg-Ettlin for participating in our user study. We thank Luis Scherer for recording the time spent on mapping avalanches in the "traditional way". We are grateful to the two anonymous reviewers and Ron Simenhois (community comment) for asking critical questions, giving suggestions and making comments for improving this work.

References

Baumer, J., Metzger, N., Hafner, E. D., Daudt, R. C., Wegner, J. D., and Schindler, K.: Automatic Image Compositing and Snow Segmentation for Alpine Snow Cover Monitoring, in: 2023 10th IEEE Swiss Conference on Data Science (SDS), pp. 77–84, https://doi.org/10.1109/SDS57534.2023.00018, 2023.

Benenson, R., Popov, S., and Ferrari, V.: Large-Scale Interactive Object Segmentation With Human Annotators, in: 2019 IEEE/CVF Conference on Computer Vision and Pattern Recognition (CVPR), pp. 11 692–11 701, https://doi.org/10.1109/CVPR.2019.01197, 2019.

Bianchi, F. M., Grahn, J., Eckerstorfer, M., Malnes, E., and Vickers, H.: Snow Avalanche Segmentation in SAR Images With Fully Convolutional Neural Networks, IEEE Journal of Selected Topics in Applied Earth Observations and Remote Sensing, 14, 75–82, https://doi.org/10.1109/JSTARS.2020.3036914, 2021.

Boykov, Y. and Jolly, M.-P.: Interactive graph cuts for optimal boundary & region segmentation of objects in N-D images, in: Proceedings Eighth IEEE International Conference on Computer Vision. ICCV 2001, vol. 1, pp. 105–112 vol.1, https://doi.org/10.1109/ICCV.2001.937505, 2001.

Bozzini, C., Conedera, M., and Krebs, P.: A New Monoplotting Tool to Extract Georeferenced Vector Data and Orthorectified Raster Data from Oblique Non-Metric Photographs, International Journal of Heritage in the Digital Era, 1, 499–518, https://doi.org/10.1260/2047-4970.1.3.499, 2012.

Bozzini, C., Conedera, M., and Krebs, P.: A new tool for facilitating the retrieval and recording of the place name cultural heritage, The International Archives of the Photogrammetry, Remote Sensing and Spatial Information Sciences, XL-5/W2, 115–118, https://doi.org/10.5194/isprsarchives-XL-5-W2-115-2013, 2013.

Bründl, M. and Margreth, S.: Integrative Risk Management, in: W. Haeberli & C. Whiteman (Eds.), Snow and Ice-Related Hazards, Risks and Disasters 2015, pp. 263–301, https://doi.org/10.1016/B978-0-12-394849-6.00009-3, 2015.

Bühler, Y., Hafner, E. D., Zweifel, B., Zesiger, M., and Heisig, H.: Where are the avalanches? Rapid SPOT6 satellite data acquisition to map an extreme avalanche period over the Swiss Alps, The Cryosphere, 13, 3225–3238, https://doi.org/10.5194/tc-13-3225-2019, 2019.

Bühler, Y., Bebi, P., Christen, M., Margreth, S., Stoffel, L., Stoffel, A., Marty, C., Schmucki, G., Caviezel, A., Kühne, R., Wohlwend, S., and Bartelt, P.: Automated avalanche hazard indication mapping on a statewide scale, Natural Hazards and Earth System Sciences, 22, 1825–1843, https://doi.org/10.5194/nhess-22-1825-2022, 2022.

Chen, L., Strauch, M., and Merhof, D.: Instance Segmentation of Biomedical Images with an Object-aware Embedding Learned with Local Constraints, 2020.

Christen, M., Kowalski, J., and Bartelt, P.: RAMMS: Numerical simulation of dense snow avalanches in three-dimensional terrain, Cold Regions Science and Technology, 63, 1–14, https://doi.org/10.1016/j.coldregions.2010.04.005, 2010.

Cronbach, L. J.: Test “reliability”: Its meaning and determination, Psychometrika, 12, 1–16, https://doi.org/10.1007/bf02289289, 1947.

De Brabandere, B., Neven, D., and Van Gool, L.: Semantic Instance Segmentation for Autonomous Driving, in: 2017 IEEE Conference on Computer Vision and Pattern Recognition Workshops (CVPRW), pp. 478–480, https://doi.org/10.1109/CVPRW.2017.66, 2017.

EAWS: Standards: Avalanche Size, https://www.avalanches.org/standards/avalanche-size/, last access: 2023-05-08, 2023.

Eckerstorfer, M., Bühler, Y., Frauenfelder, R., and Malnes, E.: Remote sensing of snow avalanches: Recent advances, potential, and limitations, Cold Regions Science and Technology, 121, 126–140, https://doi.org/10.1016/j.coldregions.2015.11.001, 2016.

Eckerstorfer, M., Vickers, H., Malnes, E., and Grahn, J.: Near-Real Time Automatic Snow Avalanche Activity Monitoring System Using Sentinel-1 SAR Data in Norway, Remote Sensing, 11, https://doi.org/10.3390/rs11232863, 2019.

ESA: DEFROST, https://business.esa.int/projects/defrost, last access 08.02.2024, 2020.

Fox, J., Siebenbrunner, A., Reitinger, S., Peer, D., and Rodríguez-Sánchez, A.: Deep Learning for Real-Time Avalanche Detection in Webcam Images, International Snow Science Workshop ISSW, Bend, 8-13 October 2023, 2023.

Golparvar, B. and Wang, R.-Q.: AI-supported Framework of Semi-Automatic Monoplotting for Monocular Oblique Visual Data Analysis, 2021.

Gulshan, V., Rother, C., Criminisi, A., Blake, A., and Zisserman, A.: Geodesic star convexity for interactive image segmentation, in: 2010 IEEE Computer Society Conference on Computer Vision and Pattern Recognition, pp. 3129–3136, https://doi.org/10.1109/CVPR.2010.5540073, 2010.

Gupta, A., Dollar, P., and Girshick, R.: LVIS: A Dataset for Large Vocabulary Instance Segmentation, in: Proceedings of the IEEE/CVF Conference on Computer Vision and Pattern Recognition (CVPR), https://doi.org/10.48550/arXiv.1908.03195, 2019.

Hafner, E. D., Techel, F., Leinss, S., and Bühler, Y.: Mapping avalanches with satellites – evaluation of performance and completeness, The Cryosphere, 15, 983–1004, https://doi.org/10.5194/tc-15-983-2021, 2021.

Hafner, E. D., Barton, P., Daudt, R. C., Wegner, J. D., Schindler, K., and Bühler, Y.: Automated avalanche mapping from SPOT 6/7 satellite imagery with deep learning: results, evaluation, potential and limitations, The Cryosphere, 16, 3517–3530, https://doi.org/10.5194/tc-16-3517-2022, 2022.

Hafner, E. D., Oberson, L., Kontogianni, T., Caye Daudt, R., Wegner, J. D., Schindler, K., and Bühler, Y.: Using interactive object segmentation to derive avalanche outlines from webcam imagery, in: EGU General Assembly Conference Abstracts, EGU General Assembly Conference Abstracts, pp. EGU–10 867, https://doi.org/10.5194/egusphere-egu23-10867, 2023.

Hafner, E. D., Techel, F., Daudt, R. C., Wegner, J. D., Schindler, K., and Bühler, Y.: Avalanche size estimation and avalanche outline determination by experts: reliability and implications for practice, Natural Hazards and Earth System Sciences, 23, 2895–2914, https://doi.org/10.5194/nhess-23-2895-2023, 2023.

He, K., Gkioxari, G., Dollár, P., and Girshick, R.: Mask R-CNN, https://doi.org/10.48550/arXiv.1703.06870, 2018.

Kapper, K. L., Goelles, T., Muckenhuber, S., Trügler, A., Abermann, J., Schlager, B., Gaisberger, C., Eckerstorfer, M., Grahn, J., Malnes, E., Prokop, A., and Schöner, W.: Automated snow avalanche monitoring for Austria: State of the art and roadmap for future work, Frontiers in Remote Sensing, 4, https://doi.org/10.3389/frsen.2023.1156519, 2023.

Karas, A., Karbou, F., Giffard-Roisin, S., Durand, P., and Eckert, N.: Automatic Color Detection-Based Method Applied to Sentinel-1 SAR Images for Snow Avalanche Debris Monitoring, IEEE Transactions on Geoscience and Remote Sensing, 60, 1–17, https://doi.org/10.1109/TGRS.2021.3131853, 2022.

Keskinen, Z., Hendrikx, J., Eckerstorfer, M., and Birkeland, K.: Satellite detection of snow avalanches using Sentinel-1 in a transitional snow climate, Cold Regions Science and Technology, 199, 103 558, https://doi.org/https://doi.org/10.1016/j.coldregions.2022.103558, 2022.

Kirillov, A., Mintun, E., Ravi, N., Mao, H., Rolland, C., Gustafson, L., Xiao, T., Whitehead, S., Berg, A. C., Lo, W.-Y., Dollár, P., and Girshick, R.: Segment Anything, https://doi.org/10.48550/arXiv.2304.02643, 2023.

Kontogianni, T., Gygli, M., Uijlings, J., and Ferrari, V.: Continuous Adaptation for Interactive Object Segmentation by Learning from Corrections, 2020.

Levandowsky, M. and Winter, D.: Distance between sets, Nature, 234, 34–35, 1971.

Li, Z., Chen, Q., and Koltun, V.: Interactive Image Segmentation with Latent Diversity, in: 2018 IEEE/CVF Conference on Computer Vision and Pattern Recognition, pp. 577–585, https://doi.org/10.1109/CVPR.2018.00067, 2018.

Lin, T.-Y., Maire, M., Belongie, S., Bourdev, L., Girshick, R., Hays, J., Perona, P., Ramanan, D., Zitnick, C. L., and Dollár, P.: Microsoft COCO: Common Objects in Context, https://doi.org/10.48550/arXiv.1405.0312, 2015.

Lin, Z., Duan, Z.-P., Zhang, Z., Guo, C.-L., and Cheng, M.-M.: FocusCut: Diving into a Focus View in Interactive Segmentation, in: 2022 IEEE/CVF Conference on Computer Vision and Pattern Recognition (CVPR), pp. 2627–2636, https://doi.org/10.1109/CVPR52688.2022.00266, 2022.

Liu, Y., Li, H., Hu, C., Luo, S., Luo, Y., and Chen, C. W.: Learning to Aggregate Multi-Scale Context for Instance Segmentation in Remote Sensing Images, 2022.

Mahadevan, S., Voigtlaender, P., and Leibe, B.: Iteratively Trained Interactive Segmentation, in: 2018 Conference on Computer Vision and Pattern Recognition (CVPR), https://doi.org/10.48550/arXiv.1805.04398, 2018.

Padilla, R., Netto, S. L., and da Silva, E. A. B.: A Survey on Performance Metrics for Object-Detection Algorithms, 2020 International Conference on Systems, Signals and Image Processing (IWSSIP), pp. 237–242, https://api.semanticscholar.org/CorpusID:220734135, 2020.

Portenier, C., Hüsler, F., Härer, S., and Wunderle, S.: Towards a webcam-based snow cover monitoring network: methodology and evaluation, The Cryosphere, 14, 1409–1423, https://doi.org/10.5194/tc-14-1409-2020, 2020.

Produit, T., Ingensand, J., and Milani, G.: QGIS plugin or web app? Lessons learned in the development of a 3D georeferencer, PeerJ Prepr., 4, e2243, https://api.semanticscholar.org/CorpusID:21774865, 2016.

R Core Team: R: A Language and Environment for Statistical Computing, R Foundation for Statistical Computing, Vienna, Austria, https://www.R-project.org/, 2021.

Redmon, J., Divvala, S., Girshick, R., and Farhadi, A.: You Only Look Once: Unified, Real-Time Object Detection, https://doi.org/10.48550/arXiv.1506.02640, 2016.

Rother, C., Kolmogorov, V., and Blake, A.: "GrabCut": Interactive Foreground Extraction Using Iterated Graph Cuts, 23, https://doi.org/10.1145/1015706.1015720, 2004.

Rudolf-Miklau, F., Sauermoser, S., and Mears, A., eds.: The technical avalanche protection handbook, Ernst & Sohn, Berlin, 2015.

Sampl, P. and Zwinger, T.: Avalanche simulation with SAMOS, Annals of Glaciology, 38, 393–398, https://doi.org/10.3189/172756404781814780, 2004.

Sofiiuk, K., Petrov, I., Barinova, O., and Konushin, A.: f-BRS: Rethinking Backpropagating Refinement for Interactive Segmentation, https://doi.org/10.48550/arXiv.2001.10331, 2020.

Sofiiuk, K., Petrov, I. A., and Konushin, A.: Reviving Iterative Training with Mask Guidance for Interactive Segmentation, https://doi.org/10.48550/arXiv.2102.06583, 2021.

Supervisely: Supervisely Computer Vision platform, https://supervisely.com, https://supervisely.com, last access 2023-07-20, 2023.

University of Innsbruck, Lo.La Peak Solutions GmbH, Avalanche Warning Service Tyrol, and Avalanche Warning Service Bavaria: UIBK Avalanche Dataset, https://doi.org/10.48323/H07F4-QZD17, 2023.

Wang, J., Sun, K., Cheng, T., Jiang, B., Deng, C., Zhao, Y., Liu, D., Mu, Y., Tan, M., Wang, X., Liu, W., and Xiao, B.: Deep High-Resolution Representation Learning for Visual Recognition, 2020.

Wesselink, D. S., Malnes, E., Eckerstorfer, M., and Lindenbergh, R. C.: Automatic detection of snow avalanche debris in central Svalbard using C-band SAR data, Polar Research, 36, 1333 236, https://doi.org/10.1080/17518369.2017.1333236, 2017.

Xu, N., Price, B., Cohen, S., Yang, J., and Huang, T.: Deep Interactive Object Selection, in: 2016 IEEE Conference on Computer Vision and Pattern Recognition (CVPR), pp. 373–381, https://doi.org/10.1109/CVPR.2016.47, 2016.

Xu, Z. and Zhao, S.: Fine-grained urban blue-green-gray landscape dataset for 36 Chinese cities based on deep learning network, Scientific Data, 11, https://doi.org/10.1038/s41597-023-02844-2, 2024.

Yuan, Y., Chen, X., and Wang, J.: Object-Contextual Representations for Semantic Segmentation, in: Computer Vision – ECCV 2020, pp. 173–190, Springer International Publishing, https://doi.org/10.1007/978-3-030-58539-6_11, 2020.